Supplement of Nat. Hazards Earth Syst. Sci., 22, 3701–3724, 2022
https://doi.org/10.5194/nhess-22-3701-2022-supplement

Natural Hazards and Earth System Sciences
Open Access
EGU

Supplement of

Meteorological, impact and climate perspectives of the 29 June 2017 heavy precipitation event in the Berlin metropolitan area

Alberto Caldas-Alvarez et al.

Correspondence to: Alberto Caldas-Alvarez (alberto.caldas-alvarez@kit.edu) and Johannes Quaas (j.quaas@uni-leipzig.de)

Supplementary Material

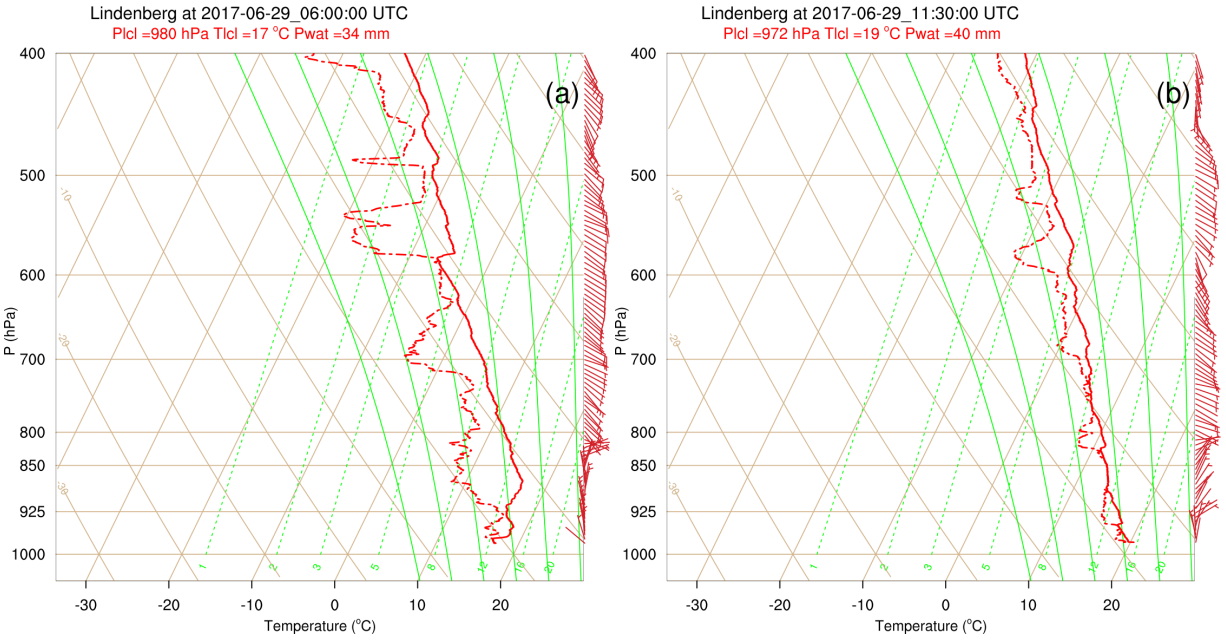

Figure S1. Radiosoundings from Lindenberg (southeast of Berlin), valid at 06 UTC (left) and 12 UTC (middle), 29 June 2017.

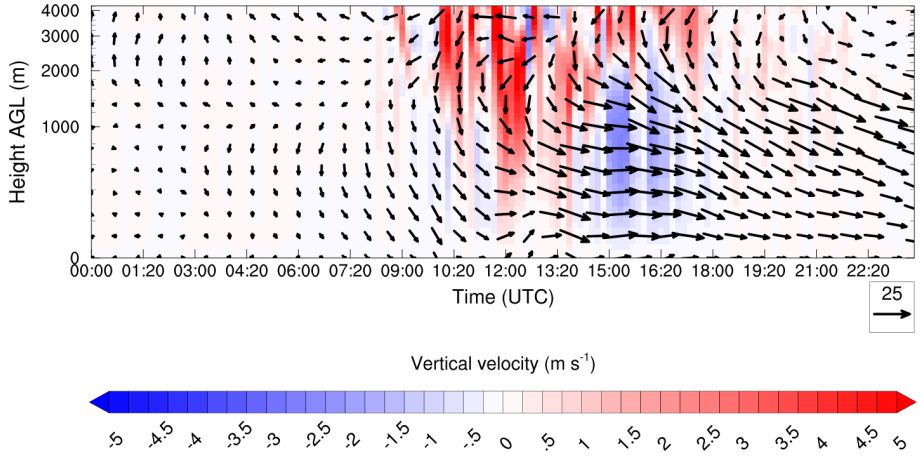

Figure S2. Time-height cross-section of simulated vertical velocities at the same location as in Fig. 4

Table S1. List of the 20 highest 24-hour precipitation totals (mm) in the federal state of Brandenburg (BB), Berlin (BE) and southern Mecklenburg-Western Pomerania (MV) on 29 June 29 2017 (DWD stations).

ID	Name	Rainfall (mm)	Coordinates
430	Berlin-Tegel (BE)	196.9	52.56°N, 13.32°E
5983	Zeesen (BB)	149.9	52.26°N, 13.62°E
2733	Kremmen-Groß Ziethen (BB)	130.6	52.73°N, 13.01°E
5307	Berge/Prignitz (BB)	124.0	53.24°N, 11.87°E
3205	Marwitz (Wasserwerk) (BB)	113.2	52.66°N, 13.18°E
3196	Marnitz (MV)	112.9	53.32°N, 11.93°E
433	Berlin-Tempelhof (BE)	112.8	52.47°N, 13.40°E
4013	Pritzwalk (BB)	110.0	53.17°N, 12.16°E
2531	Karstädt/Prignitz (BB)	109.2	53.17°N, 11.75°E
2863	Langerwisch (BB)	106.5	52.32°N, 13.07°E
4637	Staaken (BB)	106.0	52.54°N, 13.12°E
7413	Grabow-Stadt (MV)	105.4	53.28°N, 11.56°E
2779	Kuhbier (BB)	103.6	53.15°N, 12.09°E
5555	Thyrow (BB)	103.2	52.25°N, 13.24°E
2472	Jühnsdorf-Blankenfelde (BB)	103.0	52.32°N, 13.39°E
5825	Berge /BB)	102.6	52.62°N, 12.79°E
2637	Klink (MV)	100.4	53.46°N, 12.61°E
400	Berlin-Buch (BE)	99.3	52.63°N, 13.50°E
426	Berlin-Schmöckwitz (BE)	95.2	52.38°N, 13.62°E
4894	Hennigsdorf b. Berlin-Stolpe-Süd (BB)	95.0	52.63°N, 13.23°E

Comparing the return periods of the 29 June 2017 and 14 July 2021 extreme events

Here, we will discuss the 2017 extreme event in the context of the Kreienkamp et al. (2021) study as the events exhibit similarities regarding the local scale and its convective characteristic. It should be noted, however, that Kreienkamp et al. (2021) has been a rapid attribution study which has not gone through peer-review yet. The July 2021 severe precipitation at the Ahr, Erft and Meuse has been an extremely rare event – so rare that estimation of a return period for the combined Ahr and Erft catchment is challenging. Thus, a pooling approach, whereby tiles of equal size in a wider region around the event are used to estimate the return period and the impact of anthropogenic climate change on the event, was applied. Choosing such an approach was based on the assumption that the given event could have occurred anywhere in a wider region around the event. It was found that in any 130x130km tile within the wider region, one such event can be expected every 400 years, which means that several such events would occur in the wider western European region in 400 years.

To put the event we analyse here into the context of Kreienkamp et al. (2021), we compare the return periods of the events. Table S2 gives the return period of the 2017 event, spatially averaged over regions of different sizes (see also Sect. 4.3). The return period of the 2017 event, which has locally quite long return periods, decreases to 75 years when averaged over an area of 11,100 km^2 (100×111 km, yellow box in Figure 5), which is still smaller than the area size selected in Kreienkamp et al. (2021). Thus, the 2017 event has a lower return period than the 2021 event on a regional scale.

Table S2. Return period estimates for spatially averaged daily precipitation accumulation for regions of different size. The three regions (pink, grey, brown) are shown in Figure 10.

Region	Latitude [°] south corner	Latitude [°] north corner	Longitude [°] west corner	Longitude [°] east corner	Area size [km^2]	24-hour precipitation [mm]	Return period [years]
pink	52.47	52.62	13.20	13.50	340	134.5	429
grey	52.25	52.75	12.75	13.75	3.720	99.0	161
brown	52.00	53.00	12.50	14.00	11.100	75.7	75

Conditional Event Attribution

CMIP6 models and climate-change signal

The CMIP6 models from which we compute the climate-change signal are shown in Table S3. To compute the climate change signal, we first calculate the mean temperature from the CMIP6 pre-industrial simulations from 1850-1859 across all models for the months of June and July (our event occurs on 29th June) and average over the 0.11° domain (Figure S3). This is then repeated for the years 2007-2016, representative of the present climate. As the CMIP6 historical simulations end in 2014, the years 2015 and 2016 are taken from the SSP245 scenario. The actual choice of scenario here is not relevant, because the divergence between the different scenarios from 2015-2016 is trivial. The difference between the 2007-2016 and the 1850-

1859 climate is then taken. This difference is the basis for creating the pre-industrial boundary conditions from the observed boundary conditions, as described in the main manuscript.

Table S3. CMIP6 GCMs used to compute the climate-change signal used for adjusting the initial and lateral boundary conditions in the conditional event attribution study. The 17 GCMs were selected as they were the only ones for which soil temperature data were also available.

	GCM	Experiment	Institute
1	BCC-CSM2-MR	r1i1p1f1	BCC
2	FGOALS-f3-L	r1i1p1f1	CAS
3	FGOALS-g3	r1i1p1f1	CAS
4	CanESM5	r1i1p1f1	CCCma
5	CMCC-CM2-SR5	r1i1p1f1	CMCC
6	ACCESS-ESM1-5	r1i1p1f1	CSIRO
7	ACCESS-CM2	r1i1p1f1	CSIRO-ARCCSS
8	MPI-ESM1-2-HR	r1i1p1f1	DKRZ
9	EC-Earth3	r1i1p1f1	EC-Earth-Consortium
10	IPSL-CM6A-LR	r1i1p1f1	IPSL
11	MIROC6	r1i1p1f1	MIROC
12	MPI-ESM1-2-LR	r1i1p1f1	MPI-M
13	MRI-ESM2-0	r1i1p1f1	MRI
14	CESM2-WACCM	r1i1p1f1	NCAR
15	NorESM2-LM	r1i1p1f1	NCC
16	NorESM2-MM	r1i1p1f1	NCC
17	KACE-1-0-G	r1i1p1f1	NIMS-KMA

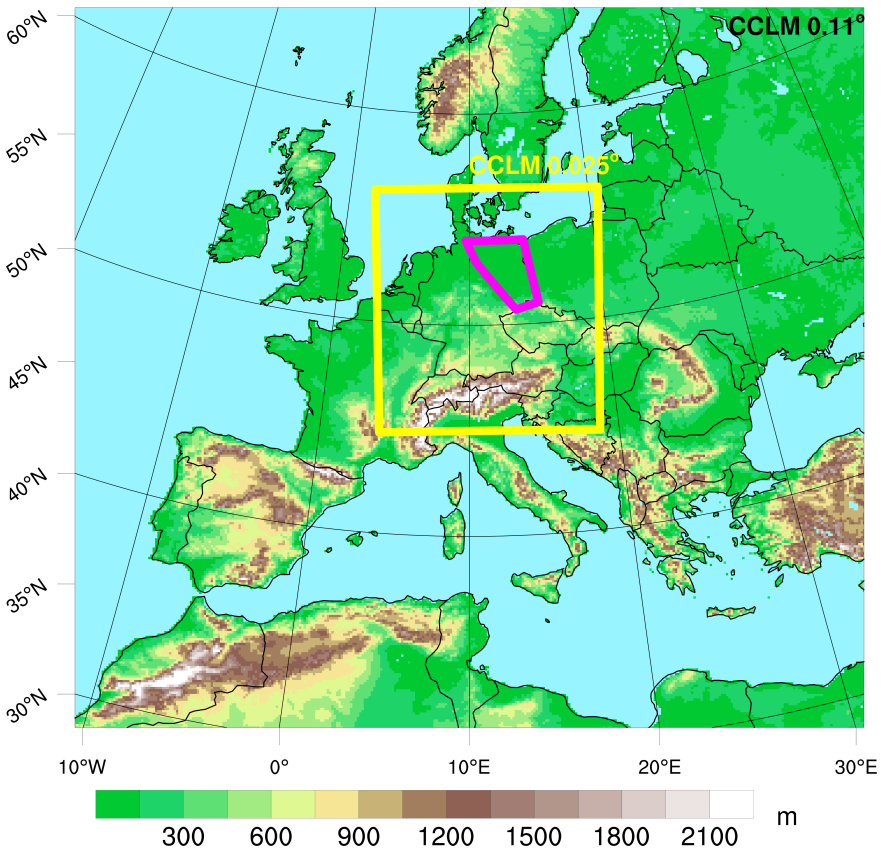

Figure S3. Central 0.11° simulation domain used in the conditional attribution study of Section 4.4 (recall from the description in the main manuscript that the ensemble is created using the domain-shift technique (Rezacova et al., 2009), whereby the boundaries and centre of the 0.11° domain are systematically shifted for each member); shading shows the orography of the 0.11° domain. The 0.025° simulation domain is marked in yellow. The magenta polygon marks the analysis region.

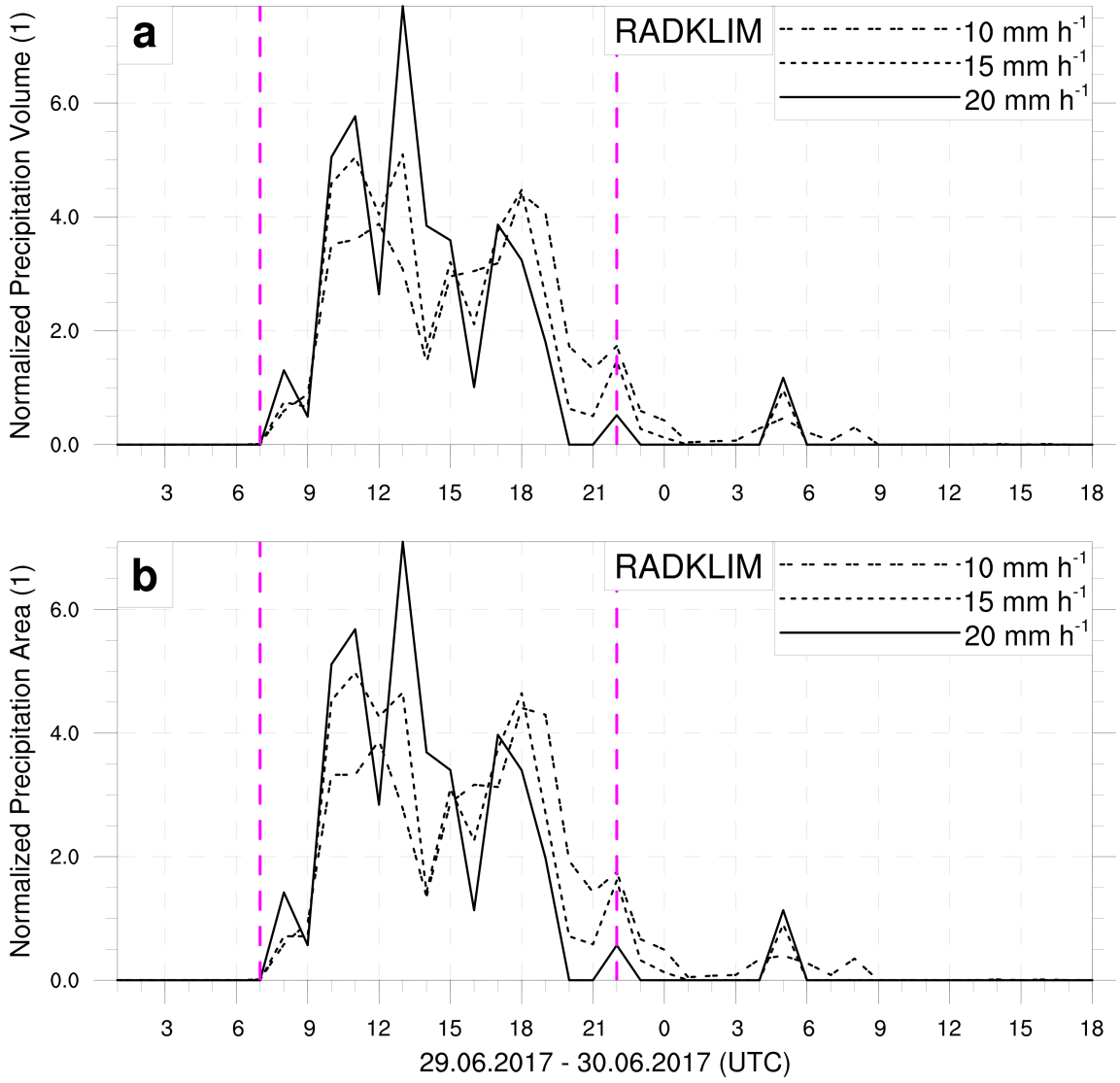

Figure S4. Normalized hourly time series of (a) precipitation volume and (b) precipitation area for different minimum precipitation intensities, based on the radar-based RADKLIM data set (Winterrath et al., 2018). The times series is based on the analysis region marked in Figures S5 and S6. The precipitation intensities denote the minimum precipitation intensities considered for each time series, i.e. for (a), the 10 mm h^{-1} line represents the total precipitation volume based on all grid cells with an hourly rate above 10 mm h^{-1}. The vertical magenta lines mark the time period (i.e. accumulation time) chosen for the analysis presented in Section 4.4 of the main manuscript and below.

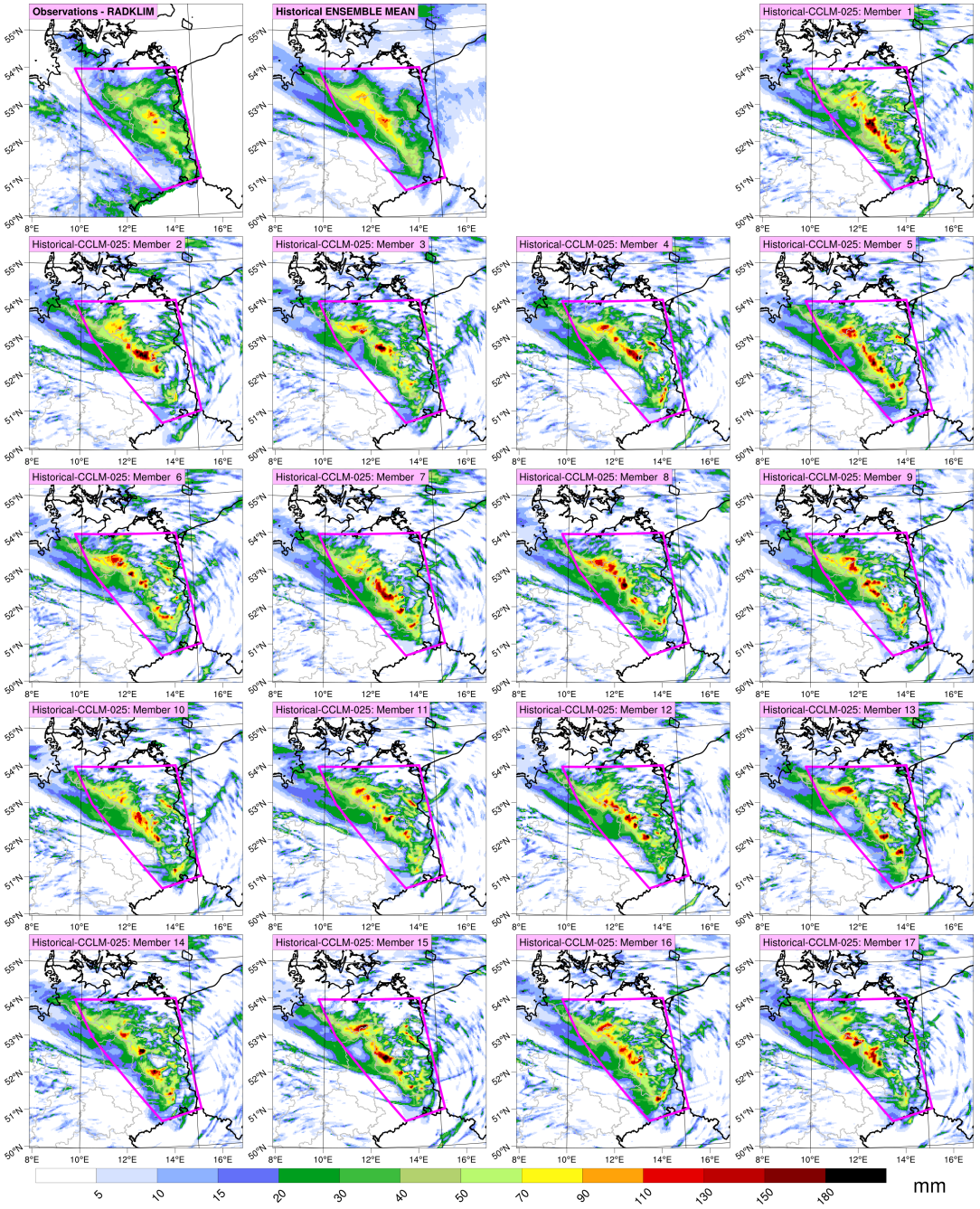

Figure S5. Pre-industrial COSMO-CLM ensemble: event total precipitation accumulations for observations (top left), ensemble mean (top, second from left) and all 17 ensemble members. The magenta box marks the analysis region used in the main manuscript. The accumulation period is as shown in Figure S4. Note that, for fair comparison, the RADKLIM data have been spatially aggregated to the COSMO-CLM 0.025° grid.

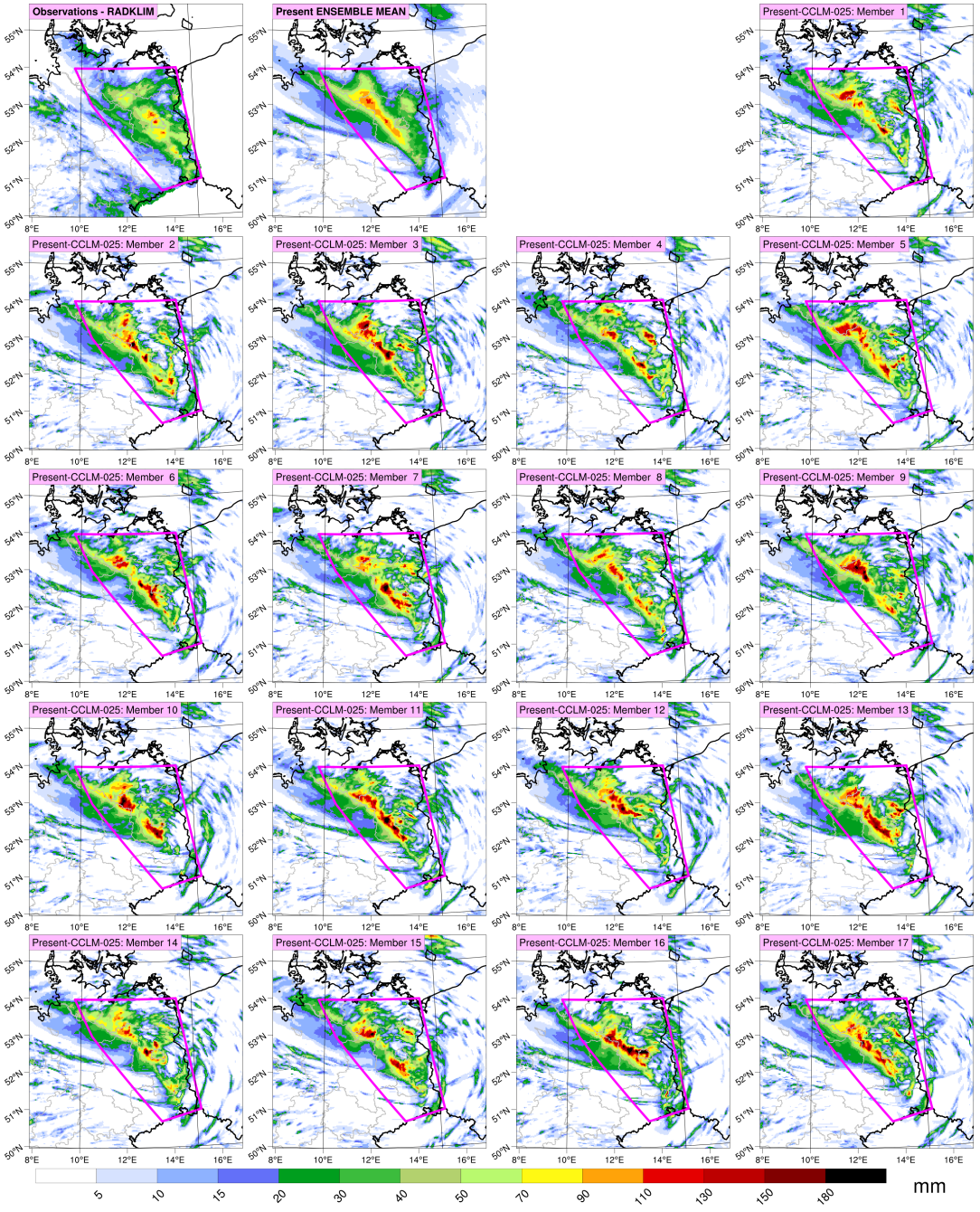

Figure S6. As in Figure S5, except for the present-climate ensemble.